Laboratory calibration for multidirectional spectroradiometers

OPEN ACCESS
IOP Publishing
Measurement Science and Technology
Meas. Sci. Technol. **32** (2021) 095902 (10pp)
https://doi.org/10.1088/1361-6501/abeb93

Laboratory calibration for multidirectional spectroradiometers

Angelika Niedzwiedz*, Jens Duffert, Mario Tobar-Foster, Esther Quadflieg and Gunther Seckmeyer

Institut für Meteorologie und Klimatologie, Leibniz Universität Hannover, Herrenhäuser Str. 2, D-30419 Hannover, Germany

E-mail: niedzwiedz@muk-uni-hannover.de

Received 4 December 2020, revised 31 January 2021
Accepted for publication 3 March 2021
Published 1 June 2021

Abstract

A method for the calibration of multidirectional spectroradiometers (MUDISs) capable of the simultaneous measurement of spectral radiance at different wavelengths is presented. The calibration of the spectroradiometer is challenging and crucial for high quality measurements of the angular dependence of the radiance. The calibration device consists of an integrating sphere (also known as Ulbrichtkugel), with a diameter of 100 cm, equipped with three 100 W lamps positioned in the lower hemisphere, with the input optics of the MUDIS directed towards the upper hemisphere. The MUDIS detects radiation from 113 different directions simultaneously in a wavelength range from 300 nm to 550 nm. Due to multiple reflections within the sphere, the radiance from the upper hemisphere is nearly homogeneous with deviations of less than 3% on average. Disregarding the 3% variability and assuming a homogeneous radiance inside the upper hemisphere of the integrating sphere, the spectral responsivities of all the MUDIS channels were determined based on the measured zenith radiance, which was detected by a pre-calibrated Network for the Detection of Atmospheric Composition Change reference spectroradiometer containing a scanning double monochromator with a unidirectional input optics. The input optics of the MUDIS contains thin fibers that should not be moved to avoid changes in the instrument's responsivity. The proposed method is therefore suited to determine the absolute responsivity of the MUDIS for all directions.

Keywords: calibration, multidirectional spectroradiometers, Ulbrichtkugel, radiance, spectral

(Some figures may appear in colour only in the online journal)

1. Introduction

At the Institute of Meteorology and Climatology of the Leibniz Universitaet Hannover a non-scanning, multidirectional spectroradiometer (MUDIS), for the measurement of solar, wavelength-dependent radiance from 113 directions simultaneously in less than 2 s, was the first to be developed worldwide (Riechelmann *et al* 2013). The spectral radiance (see DIN 5031-1 1982) can be used to derive further radiometric quantities and to describe interaction processes between solar radiation and atmospheric components such as: clouds that vary in time and spatial resolution (Hirsch *et al* 2012), aerosols (Dubovik and King 2000) and trace gases (Hönninger *et al* 2004), and for comparing with the results from radiative transfer modeling (Thomas and Stamnes 1999, Dubovik and King 2000, Hirsch *et al* 2012), as well as estimating the effect of solar radiation on humans (Seckmeyer *et al* 2013, Schrempf *et al* 2018). With the MUDIS device, it is possible to reduce the temporal uncertainties in measurements of the atmospheric variability. To ensure the quality control and quality assurance of the instrument, the MUDIS was intercalibrated with a unidirectional scanning charge-coupled device (CCD)-based spectroradiometer (SCCD) (Röder *et al* 2005,

* Author to whom any correspondence should be addressed.

Riechelmann *et al* 2013). However, this method proved to be very time-consuming and subject to many uncertainties. A first potential source of error is the unidirectional scanning measurement principle of the calibrated reference spectroradiometer and the resulting time differences between the detection of the variability of atmospheric conditions between the two instruments, as well as the movement of the optical fiber-based SCCD. In addition, possible changes can occur during transport of the pre-calibrated device from the laboratory to the measurement field. The pre-calibration also causes further uncertainties as it consists of several individual steps and devices including the primary and secondary calibrations lamps and reflection plate (Walker and Thompson 1994, Johnson *et al* 1996, Bernhard and Seckmeyer 1999, Pissulla *et al* 2009). In the method of Riechelmann *et al* (2013) one major cause of uncertainties is the change of solar spectral radiance by variable clouds. Therefore, it is plausible that a method with fewer steps would reduce the overall uncertainty. In order to avoid these measurement uncertainties, a method was developed that is based on an integrating sphere (Ulbrichtkugel (UK)) (Walker *et al* 1987). Such a sphere with a uniform inner coating of diffuse reflecting material is one of the calibration standards of radiometric spectroscopy (Walker *et al* 1987, Hanssen 2001, Butler *et al* 2003, Yu *et al* 2014, Gigahertz-Optik 2020a, 2020b) and can be used as a light source for a measuring device outside the sphere, or the input optics can be fixed inside the sphere. However, the shape and position of the optics may influence the unpolarised and homogeneous radiation field (Walker *et al* 1987). By using the integrating sphere, the method fulfills three important requirements for the calibration of measuring instruments based on multidirectional input optics:

(a) All optical channels with different directions are calibrated simultaneously and time efficiently within the integrating sphere;
(b) The input optics, which contains thin optical fibers, is not moved so that possible changes of the spectral responsivity due to bending of the fibers are avoided (Riechelmann 2014);
(c) The calibration is traceable to a calibrated primary standard.

In order to determine possible uncertainties in the distribution of the radiation field within the sphere (Hanssen 2001, Baumgartner 2013, Gălăţanu 2016) a homogeneity investigation was carried out ahead of the measurements.

2. Measurement devices

2.1. Multidirectional spectroradiometer

A MUDIS is a non-scanning spectroradiometer for simultaneous measurements of spectral sky radiance. It is based on a hyperspectral imager and measures spectral sky radiance in the wavelength range of 250–600 nm (only 300–550 nm should be used with reasonable uncertainty) in 113 different directions simultaneously with a high spectral and temporal (less than 2 s) resolution (Riechelmann *et al* 2013). The radiance is collected by a multidirectional input optics, which consists of 113 optical fibers mounted in a hemispherical dome (figure 1). All fibers of the same type are bundled and connected to the imaging Offner spectrometer lined up to a slit. After passing the optical components (collimator mirror, grid, etc) inside the spectrometer the light is detected by the 2D sensor of the UV-sensitive CCD camera. Both spectral and spatial information can be obtained from the acquired images. For further details on the working principle, see Riechelmann *et al* (2013) and Riechelmann (2014).

2.2. Integrating spheres

Two new Ulbricht spheres manufactured by Gigahertz-Optik GmbH (2015, 2020a, 2020b) were acquired for the calibration of the spectroradiometer with a multidirectional input optics. These calibration devices consist of spheres whose inner surface is uniformly coated with diffusely reflecting material, which is barium sulfate in the case of the larger sphere and OP.DI.MA (optical diffuse material) in the case of the smaller sphere (Gigahertz-Optik 2020a, 2020b). They are used to generate a diffuse homogeneous radiation field based on multiple reflections inside the sphere (Walker *et al* 1987).

2.2.1. Ulbrichtkugel (sphere) with a 100 cm diameter. This Ulbricht sphere, with a diameter of 1 m (UK100), is uniformly coated on the inside with barium sulfate, a known highly reflective material (Gigahertz-Optik 2020b). The optics of the MUDIS is inserted into the sphere by an opening at the bottom (figure 2, left). Inside the sphere there are three 100 W quartz halogen lamps with an angular distance of 120° to each other mounted at a height of about 40 cm (from the bottom). The radiation emitted by the lamps is reflected several times by the inner walls of the sphere, thus creating a largely diffuse homogeneous radiation field (figure 2, right), i.e. independent of the angle of incidence (see Walker *et al* 1987).

A barium sulfate-coated socket for the input optics, is installed under the UK100 and connected to a base plate (figure 2, left). The sphere can be moved up and down by a rope winch. The advantage of this setup is that there is no need to move the input optics of the MUDIS for the calibration. After lowering the sphere over the input optics, the UK100 is attached to the white base of the socket. With this setup, the input optics of the MUDIS is installed, fixed and centered in the integrating sphere above the three halogen lamps so that their direct radiation should be outside the field of view (FOV) of all fibers of the input optics.

2.2.2. Ulbrichtkugel (sphere) with a 5 cm diameter. For characterization measurements of the fibers, a small Ulbrichtkugel with a diameter of 5 cm (UK5) was used. The small integration sphere was constructed from the diffuser material OP.DI.MA. (Gigahertz-Optik 2020a). The UK5 has an entrance port and a round, 10 mm diameter, quartz glass

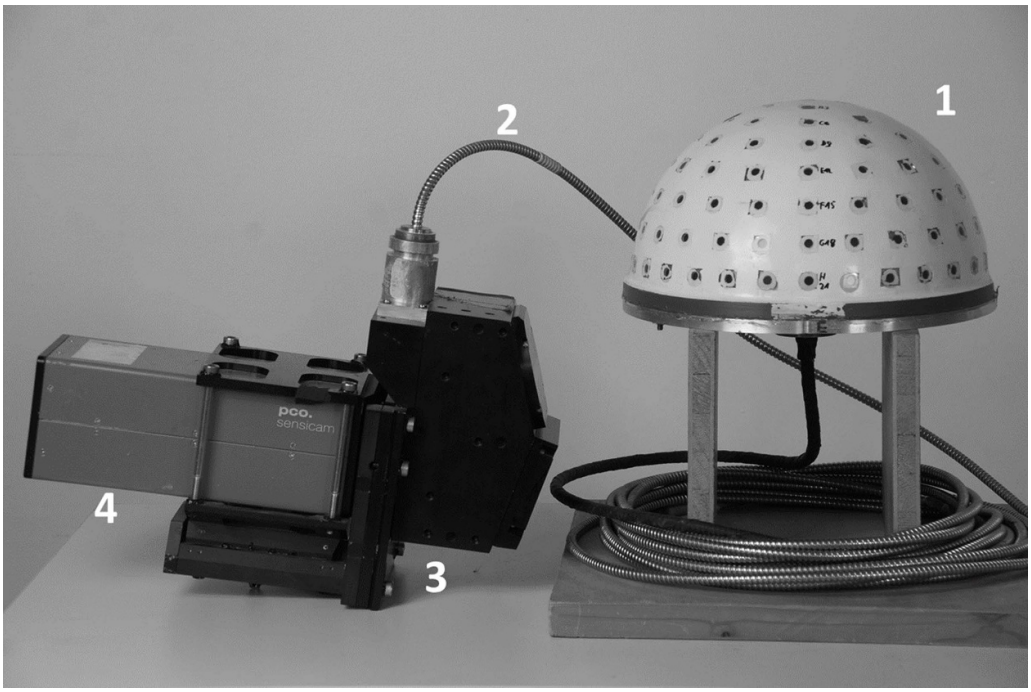

Figure 1. Picture of the MUDIS components: (1) hemispherical entrance optics dome with weather protection, (2) fiber bundle, (3) Offner imaging spectrometer, (4) UV-sensitive CCD camera (Riechelmann et al 2013). Reproduced with permission from [Holger Schilke].

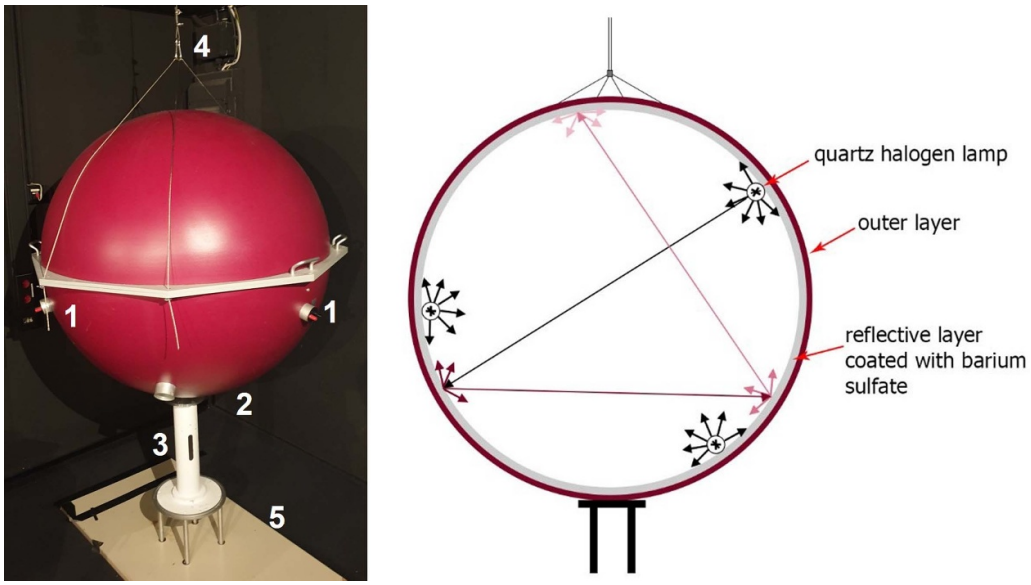

Figure 2. Left: Barium sulfate-coated Ulbricht sphere, with a diameter of 100 cm. (1) Connections for the power supplies of the three 100 W quartz halogen lamps, (2) opening at the bottom of the UK100, (3) barium sulfate-coated socket for the input optics, (4) rope winch, (5) base plate with the fixed socket. Right (front view): the radiation is reflected many times by the coating creating a diffuse radiation field within the sphere.

window aligned at 90° to it as an exit port (figure 3, left). A 0.4 mm thick optical fiber can be connected to the entrance port for directing the bundled radiation of a calibrated 100 W lamp into the UK5. An aperture at the input port prevents radiation from reaching the detector window directly. With a specially designed, mobile, aluminum adapter (figure 3, right), the constant signal of the UK5 can be measured reproducibly and individually from each fiber of the MUDIS. For this purpose, the adapter is attached to the input optics of the device and the integration sphere is reproducibly mounted on the cutouts in the adapter (figure 3, right).

3. Homogeneity analysis of the integrating sphere UK100

To ensure the comparability of the signal detected by all fibers for the absolute calibration of the MUDIS and to take into

Figure 3. Left: Integrating sphere with a 5 cm diameter consisting of: (1) quartz glass window, (2) entrance port, (3) optical fiber. Right: Mobile aluminum adapter for the MUDIS entrance optics with the connected UK5 on it.

account the variations in the radiation field due to the geometry and position of the MUDIS input optics, a homogeneity investigation of the radiation field within the UK100 was carried out in advance.

3.1. Measurement setup

In the following measurement setup, the input optics of the MUDIS was centrally installed on the barium sulfate-coated socket of the UK100 (figure 4). For the azimuthal determination of the deviations in the homogeneity, the integrating sphere was rotated around the fixed MUDIS input optics (0°–360°, in 6.9° steps). The signal inside the upper sphere was detected with eight fibers, previously characterized with the signal of the UK5 zenithally (0°–90°, in 12.8° steps). The measurements were performed at an exposure time of 360 ms and 100 averages.

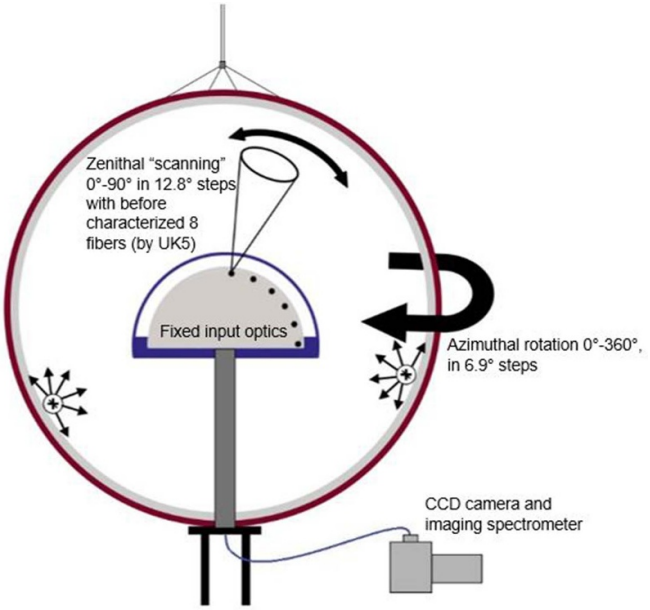

Figure 4. Sketch of the measurement principle to characterize the homogeneity of the UK100. To determine the azimuthal deviations, the UK100 was rotated in 6.9° steps by 360° around the input optics of the MUDIS (fixed inside the UK100). As a result, the diffusely radiated signal from every point of the upper hemisphere of the UK100 was detected with eight previously selected fibers (zenith directions from 0° to 90° at 12.8° intervals) of the MUDIS.

3.2. Results

The homogeneity of the radiation field of the UK100 is calculated in two steps. In the first step, the individual spectral responsivity of the fibers (Riechelmann 2014) is calculated, in order to determine the deviations (inhomogeneities) of the signal in the individual directions, by calculating the (previously performed) eight zenith measurements of the UK5 ($\mathrm{UK}_5(\vartheta, \varphi_{\mathrm{fixed}} = 0°)$, $\vartheta = 0°,\ldots, 90°$ in 12.8° steps) with the spectra recorded in the UK100 ($\mathrm{UK}_{100}(\vartheta, \varphi)$). For this purpose, the spectrum of a fiber measured for a fixed azimuth direction ($\varphi = 0° \ldots 360°$ in 6.9° steps) in the UK100 was divided by the signal of the UK5 for the corresponding fiber. This allows determination of the zenithal variations (V_Z) of the radiation field inside the UK100. The procedure was carried out for all azimuth (0°–360°) and all zenith directions (0°–90°):

$$V_Z(\vartheta, \varphi) = \frac{\mathrm{UK}_{100}(\vartheta, \varphi)}{\mathrm{UK}_5(\vartheta, \varphi_{\mathrm{fixed}} = 0°)} \quad (1)$$

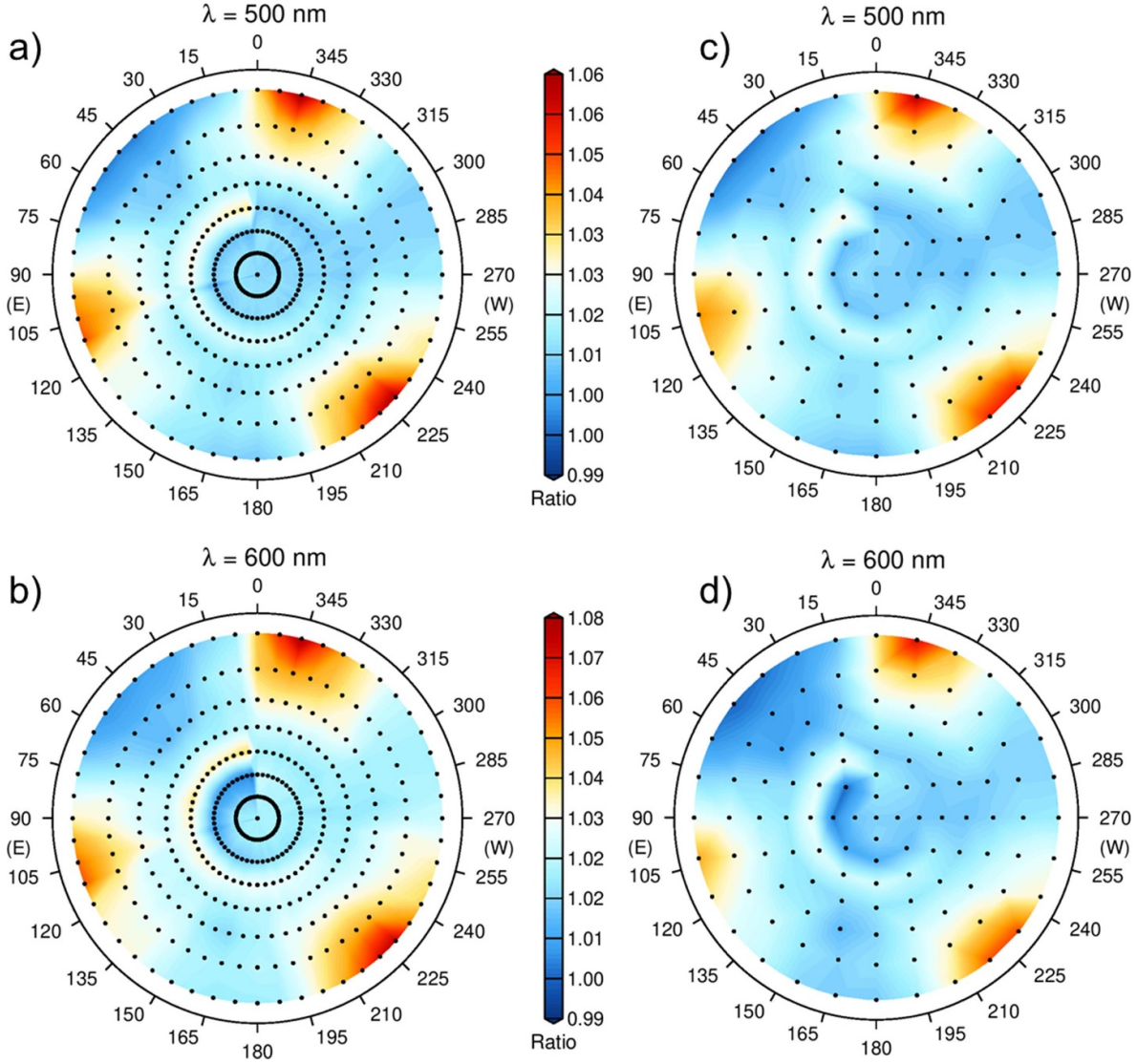

Figure 5. Ratio of spectral radiance in the upper hemisphere of the UK100 as a function of zenith and azimuth angle and spectral radiance at zenith $\vartheta = 0°$. The polar contour plot shows the remaining inhomogeneity for the wavelengths 500 nm and 600 nm. No wavelength dependence of the inhomogeneity could be determined. The position of each of the three lamps is below the horizon, but still can be identified in the values from the upper hemisphere (a)–(d). On the left side (a) and (b), the results for each measured direction are shown. The right color plot shows interpolated values using the Kriging method to the pattern (113 directions) of the MUDIS input optics (c) and (d). No major differences can be recognized between the representation on the left and the Kriging algorithm (right).

$$V_{\mathrm{Z}}(\vartheta_{\mathrm{m}},\varphi_{\mathrm{n}}) = \frac{\mathrm{UK}_{100}(\vartheta_{\mathrm{m}},\varphi_{\mathrm{n}})}{\mathrm{UK}_{5}(\vartheta_{\mathrm{m}},,\varphi_{\mathrm{fixed}}=0°)} = \begin{pmatrix} V_{\mathrm{Z}(11)} & V_{\mathrm{Z}(12)} & V_{\mathrm{Z}(13)} \\ \cdots & V_{\mathrm{Z}(22)} & \cdots \\ \cdots & \cdots & V_{\mathrm{Z}(mn)} \end{pmatrix} \quad (2)$$

with $\vartheta_{\mathrm{m}} = (1,\ldots,m)$ zenithal direction 0°–90° in 12.8° steps and $\varphi_{\mathrm{n}} = (1,\ldots,n)$ azimuthal direction 0°–360° in 6.9° steps for 1721 spectra in the range of 250–680 nm with 0.25 nm step size.

In the second step, the azimuthal dependence ($V_{\mathrm{A}}(\vartheta_{\mathrm{m}},\varphi_{\mathrm{n}})$) of the radiance within the UK100 is determined by normalizing the previously calculated spectral data ($V_{\mathrm{Z}}(\vartheta_{\mathrm{m}},\varphi_{\mathrm{n}})$) for each azimuth direction (0°–360°) to the reference spectrum of the zenith ($\mathrm{UK}_{100}(\vartheta_{\mathrm{fixed}} = 0°, \varphi_{\mathrm{fixed}} = 0°)$). Based on this calculation, the azimuthal inhomogeneity of the UK100 was determined as a function of the zenithal variations. The procedure was carried out for all azimuth (0°–360°) and all zenith directions (0°–90°):

$$V_{\mathrm{A}}(\vartheta_{\mathrm{m}},\varphi_{\mathrm{n}}) = \frac{V_{\mathrm{Z}}(\vartheta_{\mathrm{m}},\varphi_{\mathrm{n}})}{\mathrm{UK}_{100}(\vartheta_{\mathrm{fixed}}=0°,\varphi_{\mathrm{fixed}}=0°)} = \begin{pmatrix} V_{\mathrm{A}(11)} & V_{\mathrm{A}(12)} & V_{\mathrm{A}(13)} \\ \cdots & V_{\mathrm{A}(22)} & \cdots \\ \cdots & \cdots & V_{\mathrm{A}(mn)} \end{pmatrix}. \quad (3)$$

Figure 5 shows the spectral radiance of the upper hemisphere inside the UK100 in relation to the zenith and azimuth directions normalized to 0° (zenith). The measured radiance distribution was interpolated with the Kriging interpolation method (Isaak and Srivastava 1989) to the pattern

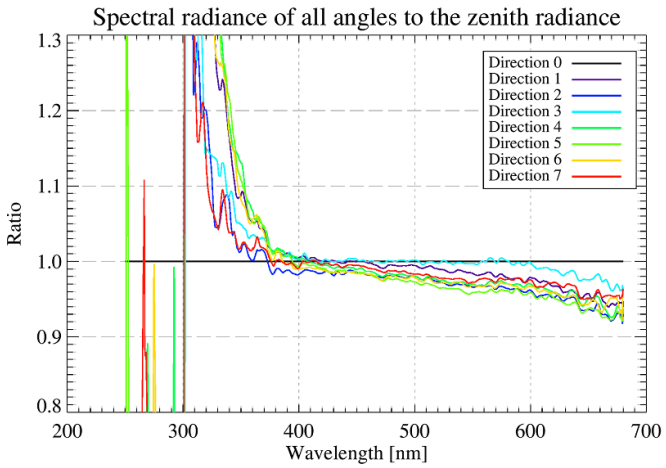

Figure 6. The ratio of the radiance of the homogeneity field in the UK100 is presented for a fixed azimuth $\varphi = 0^\circ$ and all eight measured zenith angles ($\vartheta = 0^\circ$–90°). The abscissa axis represents the wavelength range in nm. The ordinate axis is the ratio of the radiance of all directions including the zenith at ratio 1 (direction $0 = (\vartheta, \varphi) = (0^\circ, 0^\circ)$). Values lower than 300 nm are below the detection limit and are therefore random. It can be seen that the deviations to lower (<380 nm) and higher (>600 nm) wavelength ranges increase.

(113 directions) of the MUDIS input optics (c) and (d) so that the measurements in the UK100 can be corrected by a distribution function without a new characterization in the future.

The homogeneity investigations have shown that the deviations in the UK100 are generally below 3% at the wavelengths 500 nm and 600 nm in the upper hemisphere.We note that higher deviations of up to 6% occur in the emission range of the lamps near the horizon.

Figure 6 presents the ratio of the radiance of the homogeneity field inside the UK100 for a constant azimuth $\varphi = 0^\circ$ and for all eight fibers measured with a changing zenith ($\vartheta = 0$–90° in 12.8° steps, direction $0 = (\vartheta, \varphi) = (0^\circ, 0^\circ)$). It can be seen that the deviations to lower (<380 nm) and higher (>600 nm) wavelength ranges increase probably because of sensor limits and lower signal at the marginal areas of the CCD and the greater stray light impact (Riechelmann *et al* 2013). Values below 300 nm are below the detection limit and are therefore random. Especially in the UV range larger deviations were onserved due to the higher level of stray light. The deviations above 600 nm may be due to an overlap between first and second order of the grating.

Summarizing, the inhomogeneity analysis of the radiation field in the UK100 was calculated by first normalizing the measured spectra of the eight selected fibers of the MUDIS to the signal of the UK5 for a fixed azimuth direction of 0° and then applying the same procedure (equations (1)–(3)) to the zenith direction. Thus, the relative deviation of all points of the UK100 to the zenith points was calculated. For the homogeneity, absolute values were not determined; instead, the relative differences in the radiation field were investigated.

Further investigations have confirmed that the behavior is transferable to all measured azimuth directions.

4. Absolute calibration of the spectral radiance within the sphere UK100

Once the relative deviations of the spectral radiance of the upper hemisphere were established, the zenith spectral radiance was measured by another calibrated instrument. For this purpose, a calibrated scanning double monochromator system was employed. This instruments had already been used for measuring the spectral sky radiance in previous studies (e.g. Wuttke and Seckmeyer 2006, Pissulla *et al* 2009) and it is used as a reference instrument for the Network for the Detection of Atmospheric Composition Change (NDACC) (Wuttke *et al* 2006) according to the method of Meister *et al* (2002), Pissulla (2006) and Pissulla *et al* (2009).

In the first step, the direct radiation of a 1000 W working lamp was converted into diffuse and uniform radiance by a calibrated reflection plate ($L_{\mathrm{Diffusor}}(\lambda)$) (Johnson *et al* 1996, Pissulla *et al* 2009) and the spectral responsivity of the NDACC spectroradiometer ($S_{\mathrm{NDACC}}(\lambda)$) was determined (Wuttke and Seckmeyer 2006, Pissulla *et al* 2009) by

$$S_{\mathrm{NDACC}}(\lambda) = \frac{M_{\mathrm{NDACC}}(\lambda)}{L_{\mathrm{Diffusor}}(\lambda)} \tag{4}$$

where $M_{\mathrm{NDACC}}(\lambda)$ is the measured spectral signal of the reflection plate and with the units in general $[S] = \left[\frac{M}{L}\right] = \frac{\mathrm{nA}}{(\mathrm{m})\mathrm{W}\,(\mathrm{m}^2\mathrm{sr})^{-1}}$ and wavelength $\lambda = \mathrm{nm}$.

An overview of the devices used is listed in table 1.

The measurement setup and the calibration of the reference instrument (step 1) were carried out following the procedure described in Pissulla *et al* (2009), which consist of a reflection plate in combination with a secondary lamp. Uncertainties described in this reference need to be taken into account. Further uncertainties are caused by the uncertainty of the primary lamp (see table 1).The uncertainty due to voltage/current changes (Walker and Thompson 1994, Bernhard and Seckmeyer 1999) can be neglected as the lamps are operated with highly accurate power supplies, which operate the lamps at 8 ± 0.001 A. The aging of the reference standards and burning time of the lamps, which affect the emission characteristics, (Bernhard and Seckmeyer 1999) were less than 30 h.

Without moving the monochromator, in step 2, the optical fiber with the unidirectional input optics was directed from the diffusor plate to the UK100 and placed centrally in it, so that the spectral radiance of the zenith of the UK100 ($M_{\mathrm{Zenith(UK100)}}(\lambda)$) was detected using the calibrated spectroradiometer ($S_{\mathrm{NDACC}}(\lambda)$) and calculated from

$$L_{\mathrm{Zenith(UK100)}}(\lambda) = \frac{M_{\mathrm{Zenith(UK100)}}(\lambda)}{S_{\mathrm{NDACC}}(\lambda)}. \tag{5}$$

Disregarding the 3% of variation in the homogeneity of the radiation field at the wavelengths 500 nm and 600 nm in the upper hemisphere (figure 5) and assuming a nearly homogeneous radiation field inside of upper hemisphere of the

Table 1. Overview of the instruments used for the measurement of the traceability to a primary standard for the determination of the zenith radiance in the UK100. The significant components are listed with the most important technical data. Additional information can be found in the listed references or in the calibration certificates mentioned in these references.

Overview of components of the setup				
Device	Function	Characteristics	Company	References
DTMc300 double monochromator	NDACC reference device for the traceability to primary standard	2 × Czerny–Turner monochromator Wavelength: 280–2500 nm Bandwidth: 0.25 nm in the UV 1.0 nm in the VIS Entrance optic (IMUK): FOV: 4.5° Type: Optical fiber bundle	Bentham Instruments Ltd, Reading, United Kingdom IMUK	Pissulla *et al* (2009) Wuttke *et al* (2006) Wuttke and Seckmeyer (2006)
Reflection plate	Volume reflector	Size: 5 cm^2 × 10 mm Type: OP.DI.MA (optical diffuse material, here: polytetrafluoroethylene) Directional reflectance factor (DRF): R(0°/45°,λ) According to Johnson *et al* (1996) the uncertainty of 2% has to be taken into account because of the different directional reflectance factors (Gigahertz Optik:R(8°/hemispherical, λ)) Spectral reflectance: 400–1600 nm > 98% 250–2000 nm > 93%	Gigahertz-Optik GmbH	Pissulla *et al* (2009) Johnson *et al* (1996) Calibration certificate
1000 W working lamp	Secondary calibration lamp Traceability to primary standard	Type: Quartz halogen lamp, FEL Amperage: 8.0 A *Primary lamp: Type: Sylvania Amperage: 8.1 A Relative uncertainty: 270–400 nm ± 4% 420–800 nm ± 3%	Osram Gigahertz-Optik GmbH	Pissulla *et al* (2009) Bernhard and Seckmeyer (1999) Walker and Thompson (1994) *Calibration certificate

integration sphere, the spectral responsivity of all the MUDIS channels was determined as follows based on the zenith radiance.

4.1. Measurement setup

The input optics of the MUDIS is aligned and mounted centrally in the UK100 on a socket coated with barium sulfate at a height of 43 cm above the three lamps (figure 7). By switching on the three 100 W quartz halogen lamps, multiple reflections are caused by the barium sulfate coating of the sphere and a diffuse radiation field is created around the optics. The measurements were performed at an exposure time of 400 ms and 100 averages.

4.2. Results

The calculated spectral responsivity of all 113 fibers of the MUDIS ($S_{\mathrm{MUDIS,lab}(\lambda)}$) on average is shown in figure 8. This analysis used the measured spectra of the MUDIS ($M_{\mathrm{MUDIS,UK100}}(\lambda)$, measured in counts) and equation (6)) with the known radiance of the UK100 ($L_{\mathrm{Zenith(UK100)}}(\lambda)$) (equation (5)) which was determined in the first part of the measurements with the NDACC device:

$$S_{\mathrm{MUDIS,lab}}(\lambda) = \frac{M_{\mathrm{MUDIS,UK100}}(\lambda)}{L_{\mathrm{Zenith(UK100)}}(\lambda)}. \tag{6}$$

As can be seen in figure 8, the maxima of the measured spectra are between 450 and 550 nm and achieve up to 14.72 counts · (m^2 sr nm) · mW^{-1} at 446.25 nm (23.31% relative standard deviation (RSD)) on average. The minimum average value is 0.081 counts · (m^2 sr nm) · mW^{-1} at 285.50 nm. It can be observed that the RSD increases towards the marginal areas of the sensor. The high RSD at 285.50 nm may be due to the marginal areas, stray light impact and the difficulty to detect signal in the UV. The standard deviation of the maxima is up to 3.45 counts · (m^2 sr nm) · mW^{-1} at 444.75 nm. At lower (<420 nm) and higher (>500 nm) wavelengths the signal decreases. The minimum of the standard deviation is ±0.19 counts · (m^2 sr nm) · mW^{-1} at 285 nm. Generally, the wave-like shape of the measured spectra occurs in all fibers and is attributed to the device properties of the MUDIS.

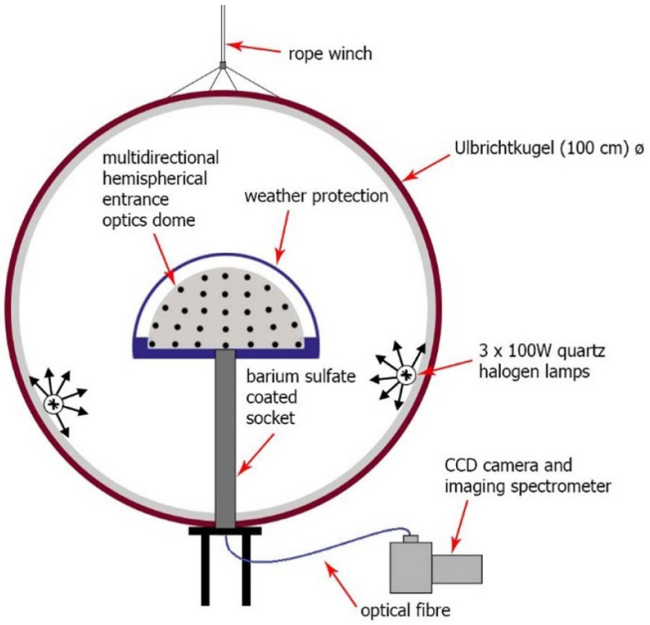

Figure 7. Measurement setup of the absolute calibration. The MUDIS is mounted centrally and fixed in the UK100 on the barium sulfate-coated socket. The multiple reflections within the UK100 cause a diffuse radiation field around the measurement optics generated by the three 100 W quartz halogen lamps and the barium sulfate coating of the sphere.

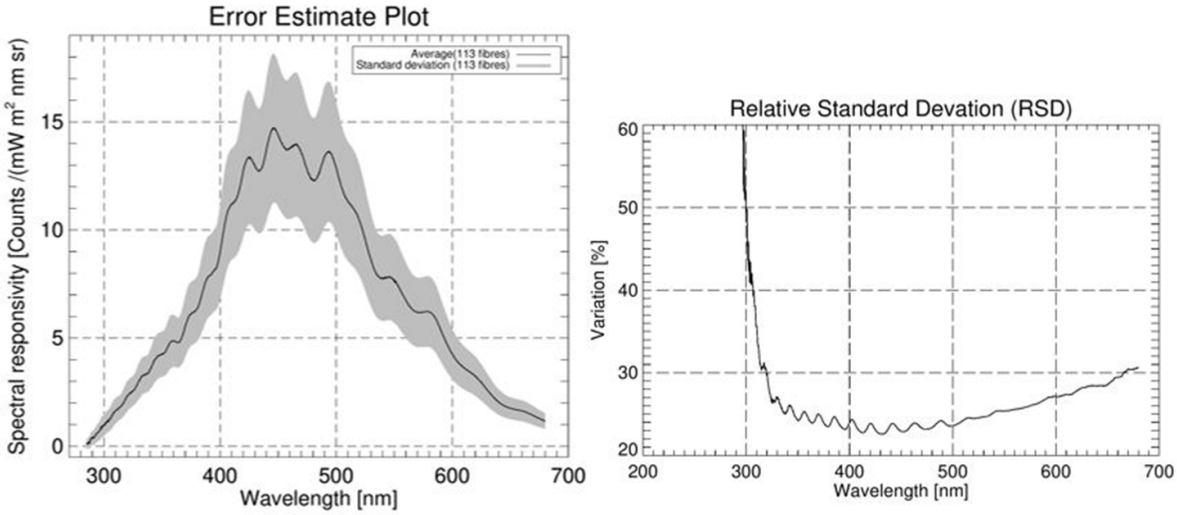

Figure 8. Left: The graph shows the spectral responsivity (black) and its standard deviation (grey area) of all 113 directions of the MUDIS on average responsivity in the UK100 with corrected stray light. Although there are deviations in the responsivity between the various directions, the relative responsivity function is similar. The maximum responsivity is between 400–550 nm, while the MUDIS is not sensitive in the UV. Right: This graph illustrates the relative standard deviation (RSD). For significant wavelengths, the RSDs are: at 320 nm = 29.8%, at 450 nm = 22.9% and at 600 nm = 27.2%.

5. Discussion and conclusion

The scientific goal of this study was to develop a method for the calibration of MUDISs capable of the simultaneous measurement of spectral radiance. With the assumption of a homogeneously distributed radiation field within an Ulbricht sphere, the individual spectral responsivity of the MUDIS can be determined simultaneously using an integrating sphere with a diameter of one meter. This method significantly improves the calibration processing compared to the UK5 integrating sphere, which is limited by the signal to noise ratio and requires very long integration times, especially in the UV range. However, the impact of the position of the three 100 W lamps inside the UK100 can be seen in the measurements

despite the fact that the input optics is located outside the FOV of the direct emission of the lamps. A possible improvement may be to shield the horizon from the direct radiation of the lamps by additional apertures in the sphere because the MUDIS fibers (Riechelmann *et al* 2013) are probably still too close to the direct emission area of the lamps. One disadvantage of calibrating with the UK100 is the decrease of the spectral reflectance of the coating due to ageing processes and the possible crumbling of the powder caused by the movement of the sphere during assembly and disassembly.

For the measurements of the traceability to a primary standard of the reference zenith radiance inside the UK100, a unidirectional input optics was used, which does not correspond to the geometry and coating of the MUDIS input optics. Therefore, the radiation field in the sphere may differ from the condition where the MUDIS input optics is within the sphere. Compared to the method of Riechelmann *et al* (2013) and the traditional calibration method (e.g. Pissulla *et al* 2009), the procedures have the common traceability to a primary standard with the possible sources of uncertainty listed in section 4 (step 1). The resulting spectral sensitivity and its dependence with the direction correspond qualitatively well with the indirect calibration method shown in Riechelmann *et al* (2013) and Riechelmann (2014). A complete analysis of the uncertainty budget, such as the one performed by Bernhard and Seckmeyer (2013) is presently beyond the possibilities and scope of this description of a new calibration method. However, the uncertainty of the new calibration with the sphere is likely smaller than the uncertainty of the indirect method used by Riechelmann *et al* (2013) because it does not depend on unstable and rapidly changing outdoor conditions (e.g. variability of clouds effects) and all channels are calibrated simultaneously without movement of the device.

Acknowledgments

We thank Holger Schilke and Ullrich Meyer for technical support. We also thank Stefan Riechelmann and Ansgar Stührmann for their support during the planning phase.

ORCID iD

Angelika Niedzwiedz https://orcid.org/0000-0002-2115-379X

References

Baumgartner A 2013 Characterization of integrating sphere homogeneity with an uncalibrated imaging spectrometer *5th Workshop on Hyperspectral Image and Signal Processing: Evolution in Remote Sensing (WHISPERS)* (Gainesville, FL) pp 1–4

Bernhard G and Seckmeyer G 1999 Uncertainty of measurements of spectral solar UV irradiance *J. Geophys. Res. Atmos.* **104** 14321–45

Butler J J *et al* 2003 Radiometric measurement comparison on the integrating sphere source used to calibrate the moderate resolution imaging spectroradiometer (MODIS) and the Landsat 7 enhanced thematic mapper plus (ETM+) *J. Res. Natl Inst. Stand. Technol.* **108** 199-228

DIN 5031 Teil 1 1982 *Strahlungsphysik Im Optischen Bereich Und Lichttechnik* (Berlin: Beuth Verlag GmbH)

Dubovik O and King M D 2000 A flexible inversion algorithm for retrieval of aerosol optical properties from Sun and sky radiance measurements *J. Geophys. Res. Atmos.* **105** 20673–96

Gălăţanu C D 2016 Geometry influence on the precision of light flux measurement with Ulbricht integrating sphere pp 604–8

Gigahertz-Optik 2015 Produkte und Dienstleistungen zur Lichtmessung (Türkenfeld: Gigahetz-Optik GmbH) (available at: www.gigahertz-optik.de/) (Accessed 15 January 2015)

Gigahertz-Optik 2020a UPK-50-L, ODM Material (Spezifikation), 6.1 Theorie der idealen Ulbrichtkugel (Türkenfeld: Gigahertz-Optik GmbH) (available at: www.gigahertz-optik.de/de-de/produkt/UPK-50-L) (Accessed 20 May 2020)

Gigahertz-Optik 2020b UMTB-1000 (Türkenfeld: Gigahertz-Optik GmbH) (available at: www.gigahertz-optik.de/de-de/produkt/UMTB-1000) (Accessed 4 December 2020)

Hanssen L 2001 Integrating-sphere system and method for absolute measurement of transmittance, reflectance, and absorbance of specular samples *Appl. Opt.* **40** 3196–204

Hirsch E, Agassi E and Koren I 2012 Determination of optical and microphysical properties of thin warm clouds using ground based hyper-spectral analysis *Atmos. Meas. Tech.* **5** 851–71

Hönninger G, Von Friedeburg C and Platt U 2004 Multi axis differential optical absorption spectroscopy (MAX-DOAS) *Atmos. Chem. Phys.* **4** 231–54

Isaak E H and Srivastava R M 1989 *An Introduction to Applied Geostatistics* (Oxford: Oxford University Press)

Johnson C, Bruce S, Early E, Houston J, O'Brian T, Thompson A, Hooker S and Mueller J 1996 The fourth Seawifs Intercalibration Round-Robin Experiment (sirrex-4) *Technisches Memorandum 37* (Greenbelt, MD: NASA Goddard Space Flight Center)

Meister G, Abel P, McClain C, Barnes R, Fargion G, Cooper J, Davis C, Korwan D, Godin M and Maffione R 2002 The first Simbios Radiometric Intercomparison (simric-1) *Technischer Report* (Greenbelt, MD: NASA Goddard Space Flight Center)

Pissula D 2006 Development of instrumentation measuring sky radiance *Diplomarbeit* Institut für Meteorologie und Klimatologie, Gottfried Wilhelm Leibniz Universität Hannover

Pissulla D *et al* 2009 Comparison of atmospheric spectral radiance measurements from five independently calibrated systems *Photochem. Photobiol. Sci.* **8** 516–27

Riechelmann S 2014 Simultaneous measurement of spectral sky radiance: development, characterization and validation of a non-scanning multidirectional spectroradiometer (MUDIS) *Dissertation* Institut für Meteorologie und Klimatologie, Gottfried Wilhelm Leibnitz Universität Hannover

Riechelmann S, Schrempf M and Seckmeyer G 2013 Simultaneous measurement of spectral sky radiance by a non-scanning multidirectional spectroradiometer (MUNDIS) *Meas. Sci. Technol.* **24** 8

Röder A, Kuemmerle T and Hill J 2005 Extension of retrospective datasets using multiple sensors an approach to radiometricnintercalibration of landsat TM and MSS data *Remote Sens. Environ.* **95** 195–210

Schrempf M, Thuns N, Lange K and Seckmeyer G 2018 Einfluss der Verschattung auf die vitamin-D-gewichtete UV-Exposition eines Menschen *Akt Dermatol.* **44** 204–9

Seckmeyer G, Schrempf M, Wieczorek A, Riechelmann S, Graw K, Seckmeyer S and Zankl M 2013 A novel method to calculate solar UV exposure relevant to vitamin D production in humans *Photochem. Photobiol.* **89** 974–83

Thomas G and Stamnes K 1999 *Radiative Transfer in the Atmosphere and Ocean* (New York: Cambridge University Press)

Walker J H and Thompson A 1994 Improved automated current control for standard lamps *J. Res. Natl Inst. Stand. Technol.* **99** 255

Walker J, Saunders R, Jackson J and McSparron D 1987 Nbs measurement services: spectral irradiance calibrations. Nbs special publication sp250-1 Center of Radiation Research, National Measurement Laboratory, National Bureau of Standards, U.S.Department of Commerce

Wuttke S and Seckmeyer G 2006 Spectral radiance and sky luminance in Antarctica: a case study *Theor. Appl. Climatol.* **85** 131–48

Wuttke S, Seckmeyer G, Bernhard G, Ehramjian J, McKenzie R, Johnston P and O'Neill M 2006 New spectroradiometers complying with the NDSC standards *J. Atmos. Ocean. Technol.* **23** 241–51

Yu X, Sun Y, Fang A, Qi W and Liu C 2014 Laboratory spectral calibration and radiometric calibration of hyper-spectral imaging spectrometer *The 2014 2nd Int. Conf. on Systems and Informatics (ICSAI 2014)* pp 871–5